Silicon (2020) 12:1145–1156
https://doi.org/10.1007/s12633-019-00201-w

ORIGINAL PAPER

Role of Oxygen Potential and Oxygen Ions on Phosphorus Removal from Silicon *via* Addition of FeO into Slag

Nan Zhang [1,2] · Guoyu Qian [1] · Zhi Wang [1] · Kuixian Wei [3] · Wenhui Ma [3] · Wei Gong [2]

Received: 5 March 2019 / Accepted: 31 May 2019 / Published online: 22 June 2019

Abstract

In present work, the role of the oxygen potential (P_{O2}) and oxygen ion (O^{2-}) concentration for removing phosphorus (P) during $CaO–SiO_2–Al_2O_3–Fe_xO$ slag refining was studied by on-line measurement of oxygen activity in molten silicon (Si), FactSage calculation, Raman spectroscopy and nuclear magnetic resonance (NMR) spectroscopy. The results show that the addition of FeO from 0 to 9.25 wt% in slag can increase the activity of dissolved oxygen ($a_{[O]}$) in Si and the mole fraction of O^{2-} in slag. Moreover, the increase of O^{2-} concentration leads to the increase of non-bridge oxygen (NBO). The value of L_P (the partition ratio of phosphorous between slag and Si shows a first increase and then decrease trend and reaches a maximum value of 1.95 at 5 ± 0.1 wt% FeO. It is believed that the increase of $a_{[O]}$ and NBO can promote the removal of P as FeO content is less than 5 ± 0.1 wt%. the chain structure unit (Q^2) of silicate network as the main intermediate structure to capture PO_4^{3-} from the charge compensation of P_2O_5 by O^{2-} to form the sheet structure unit Q^3(Si and P). When FeO content is increased to more than 5 ± 0.1 wt%, L_P value gradually decreases although the values of NBO and $a_{[O]}$ are increasing. NBO plays a leading role in this process, it can be speculated that more NBO can depolymerize the Q^3 (Si and P) to destroy the stability of P in silicate network. As a result, a mount of PO_4^{3-} is present at the interface to prevent the oxidation of phosphorous, which leads to the decrease of L_P value.

Keywords Solar grade silicon · Slag refining · P removal · Oxygen potential · Raman and NMR spectroscopy

1 Introduction

Si is the majority of PV (photovoltaic) cells [1], and the current Si feedstock costs contribute up to 25% to the direct module costs, already as a result of the starting feedstock shortage scenario [2]. However, the total quantity of 68% of Si feedstock that is lost in various forms of Si containing waste during the PV production chain, where more than 40% of the high-purity Si is wasted by slicing of wafers using a wire sawing process [3]. The recycling of the Si kerf loss can be considered as a cost-effective, circular economical solution for an advanced low-cost Si-based PV, which has received lots of attention [4]. Although the kerf loss Si particles remain in high purity, it is noteworthy that the P content in Si particles increases significantly (about dozens to hundreds of parts per million (ppm)) because of the contamination of electroplating solution containing pyrophosphate on diamond wire saw [5–8], which limits the use of recycled Si powder as Si feedstock. Many studies have been carried out on the yield of Si powder, the removal of SiC Particles, Al_2O_3, Fe_2O_3 et al [9–11]. In addition, vacuum refining such as vacuum electron beam and plasma can effectively remove P [12, 13], but it will increase the cost of Si powder recovery. Slag refining will be an effective way to remove P from regenerated Si due to the low cost and mature foundation of industrialization.

However, the low P distribution coefficient between slag and Si is a key problem in slag refining, the distribution coefficient of P, for example, is a fraction to a few tenths of boron.

Guoyu Qian and Nan Zhang Thurmond are co-first authors.

✉ Zhi Wang
zwang@ipe.ac.cn

[1] Key Laboratory of Green Process and Engineering, National Engineering Laboratory for Hydrometallurgical Cleaner Production Technology, Institute of Process Engineering, Chinese Academy of Sciences, Beijing 100190, People's Republic of China

[2] Ferrous Metallurgy Department in School of Metallurgy, Northeastern University, ShenyangLiaoning province, 110819, People's Republic of China

[3] Faculty of Metallurgical and Energy Engineering, Kunming University of Science and Technology, KunmingYunnan province, 650093, People's Republic of China

According to reactions (1) and (2), the removal of phosphorous from Si is charged by two steps. Firstly, phosphorous is oxidized to P_2O_5 at the interface between molten slag and Si, and then P_2O_5 combines with O^{2-} and go into slag in the form of PO_4^{3-}. Therefore, it is necessary to understand the effects of the oxygen potential, the concentration of O^{2-} and the stability of oxidation products with the aim of high degree of dephosphorization.

$$[P] + \frac{5}{4}O_2 = \frac{1}{2}P_2O_5 \quad (1)$$

$$\frac{1}{2}P_2O_5 + \frac{3}{2}O^{2-} = PO_4^{3-} \quad (2)$$

Many researchers have investigated how to increase the oxygen potential, for example, Monokama et al [14] and Tanahashi et al [15] have introduced the methods of controlling oxygen atmosphere and injecting oxygen gas into the molten Si. Besides, adjusting slag composition like increasing the SiO_2 activity or adding oxides such as Al_2O_3, TiO_2 to the slag can also promote the oxygen potential [16, 17]. However, only increasing the oxygen potential does not always increase the efficiency of dephosphorization, even blowing oxygen can easily cause a large loss of Si. Therefore, it is necessary to comprehensively consider the impact of other factors. As mentioned above that the concentration of O^{2-} also determines the removal efficiency of P. Adding basic oxides such as CaO, ZnO, Na_2O, MgO to the slag is a good way to increase the concentration of O^{2-} [18–20]. For the conventional slag design, the increase of oxygen potential and O^{2-} concentration has been achieved by adding the oxides with a single action, which could aggravate the complexity of the system. It is well known that FeO can improve the oxidation of slag as well as provide O^{2-}. Hence, FeO can be considered to be a good choice for adjusting slag composition. There have been a number of studies on the effect of FeO for dephosphorization during the steel-making process [21–23]. It is demonstrated that the partition ratio of phosphorous between slag and molten steel has a greater dependence on the FeO content. However, much less refining slags containing FeO is available in Si refining. This paper will conduct relevant researches on Si refining using slags with FeO.

As mentioned above, the increase of oxygen potential cannot achieve the continuous removal of phosphorous, indicating that the stability of phosphorous in slag must play an important role in P removal. The structure and existence of P in slag is an important way to investigate its stability. In existing studies, the activities of $xCaO{\cdot}P_2O_5$, $xMgO{\cdot}P_2O_5$ and $xBaO{\cdot}P_2O_5$ etc. [24–26], based on molecular theoretical model are generally used to describe the stability of P oxidation products in the slag. However, much less structural information associate with the refining behavior is available. Therefore, the relationship between the structural information and refining process are critical for the design of refining slag.

SiO_2 is the basic component of refining slag for Si, and it as an acid oxide can form a network structure. Thus, the silicate network is the basis of the coordination environment in slag. P_2O_5 as a network formation can be combined with silicate network and be fixed in slag. Therefore, an important prerequisite for the combination of phosphate and silicate is that SiO_2 and P_2O_5 are charge compensation by oxygen ions. However, enough oxygen ions can depolymerize the network, which can worsen the binding of phosphate and silicate networks [27, 28]. Therefore, oxygen ion has a great influence on the existence form of phosphate silicate network. With the assistance of Raman, NMR and FTIS spectroscopy, the network of silicate could be determined. Recently, Qian et al [27] and Morita et al [28] have revealed the role of slag structures on the removal of boron and sulfur, respectively. The behavior of boron can be investigated according to the Raman shifts of different Si–O units, namely, Q^n (Si, $n = 0$~4) [29–32]. Likewise, the P could incorporate with silicate structures through P-O-Si bonds [33] or only in the form of orthophosphate [34], which was independent in the silicate network. Previous studies mainly studied how the varying P_2O_5 content influenced the structures or physicochemical properties of phosphosilicate glass. However, detailed studies on the phosphorous removal according to the complex behavior of phosphorous in silicate network, especially for the influence of Fe_xO, were not yet fully understood.

In the present work, an attempt was made to understand the role of FeO on phosphorous removal based on comparison between experimental results of slag treatment and structural analysis of the slag. FeO was selected to change the oxygen potential and the concentration of O^{2-}. The behavior of phosphorous in the silicate network and the state of phosphorous in the slag were investigated using Raman and ^{31}P NMR spectroscopy to evaluate the stability of P in slag. Slag treatment was carried out under condition of different FeO content. The results can provide more information for the optimization of slag system.

2 Experimental

2.1 Slag Preparation

The sample required for the experiment was selected from analytical reagent grade CaO (99.0 wt% purity metal basis), SiO_2 (99.5wt%t purity metal basis), $FeC_2O_4{\cdot}2H_2O$ (99.30 wt% purity metal basis). CaO-SiO_2 system was as base slags, and $FeC_2O_4{\cdot}2H_2O$ was used to make FeO by Heating to 1273 K and keeping warm for 30 min in a tube furnace at 1273 K under argon atmosphere. To prove that FeO can be

obtained by the thermal decomposition $FeC_2O_4{\cdot}2H_2O$, the samples of heated $FeC_2O_4{\cdot}2H_2O$ was analyzed using an X-ray (XRD, SmartLab, Rigaku, Tokyo) diffractometer, as shown in Fig. 1, FeO does exist.

Five slags were set with same binary basicity (CaO/SiO_2 = C/S) 1 and different $FeC_2O_4{\cdot}2H_2O$ contents (0, 12.5, 18.7, 25 and 31.3 wt%). Just very little phosphorous come into slag after refining, which lead to a difficulty for chemical analysis of phosphorous. The study of Wang et al [33] showed that the glass network structure became more and more polymerized when the P_2O_5 content increased from 0~10 wt% in the slags, but had no effect on the type of the structure. Therefore, 5 wt% P_2O_5 was added into the $CaO–SiO_2–Fe_xO$ slags to study the behavior and structure of P from Si. P oxide was selected from analytical reagent grade P_2O_5 (99.0 wt% purity metal basis), and the treatment of the slags containing P_2O_5 was the same with above.

The fully blended samples were placed in corundum crucibles to heat to 1823 K at 10 K/min in Ar gas using muffle furnace, and then hold for two hours to make the slags be homogeneous. Subsequently, the corundum crucibles containing the molten slags were quickly quenched in liquid nitrogen to maintain the high temperature structure of slag. The quenched solid slags were broken and crushed to a powder in agate mortar. The powder was sieved to 74 μm using 200 mesh sieve and sent for X-ray fluorescence (XRF; Axios, PANalytical, Netherlands) verification of composition, as shown in Table 1. It is noteworthy that about 6~8 wt% Al_2O_3 was found in the slag due to the high temperature erosion of corundum crucibles.

In addition, a part of powder slags (No: 1, 3, 5, 1#, 3#, 5#) was also analyzed using X-ray diffractometry (XRD; SmartLab, Rigaku, Japan) to confirm the glassy nature of all samples. Figure 2 clearly shows no crystals in the slags, indicating it can be used to make an investigation of structure.

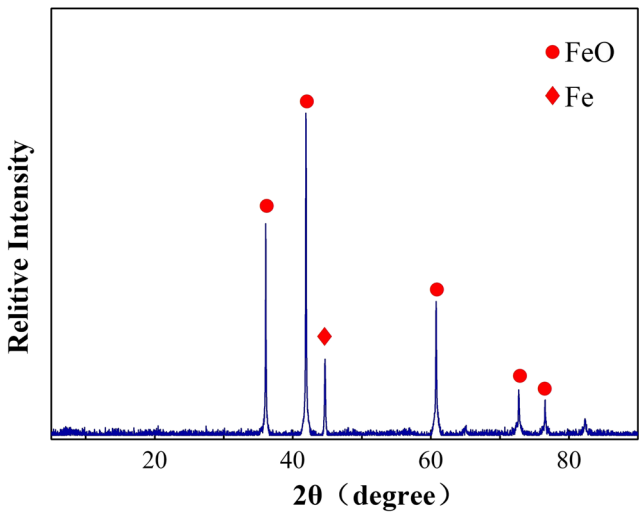

Fig. 1 XRD Patterns of $FeC_2O_4{\cdot}2H_2O$ after Heating at 1273 K

Table 1 Pre-melting slag components, as determined from X-ray fluorescence analysis, wt%

Slag	No.	CaO	SiO_2	Al_2O_3	Fe_xO	P_2O_5
Without P_2O_5	1	47.27	46.04	6.69	0	0
	2	45.20	44.44	7.50	2.86	0
	3	41.47	40.77	8.98	8.78	0
	4	39.82	38.87	8.67	12.64	0
	5	38.87	38.06	8.56	14.51	0
With P_2O_5	1#	44.17	43.02	7.89	0	4.92
	3#	42.56	41.85	8.01	8.73	4.85
	5#	36.93	36.17	8.23	13.5	5.17

The presence of small amounts of oxygen at high temperatures is unavoidable even with the protection of argon, thus some FeO could be oxidized to Fe_2O_3 [21–23]. To determine the ratio of FeO and Fe_2O_3 more precisely, the valence of Fe in slag was performed by means of X-ray Photoelectron Spectrum (ESCALAB, 250Xi). The results are presented in the following sections.

2.2 Slag Refining and Determination of Oxygen Potential

The P content of the refined silicon would be reduced sharply to very low levels, moreover, the low concentration of P in metallurgical grade-Si (MG-Si) used for refining was difficult for ICP-MS analysis. Therefore, the P content in silicon was increased by adding 1000 ppm P to the MG-Si raw material. 100 g of MG-Si was used to melt at an electromagnetic induction furnace and 0.1 g P was added in the corundum crucibles at 1823 K protected by argon atmosphere. P was evenly distributed in Si by electromagnetic stirring. After holding at 1823 K for one hour, the furnace was cooled down to room temperature at 10 K/min. The content of P in the doped Si before slag refining tested by ICP-MS was quantified to be 282 ppm (the average value from three different part of Si).

Five pre-melting slags containing different FeO content with the same CaO/SiO_2 ratio of 1 were subjected to the slag refining process. 5 g of doped Si and 15 g slag were charged into corundum crucibles for each experiment, and the crucibles were heated at 1823 K and held for two hours to stabilize the temperature in an electric resistance furnace under Ar atmosphere. Before heating, the furnace was vacuumed to 0.1 MPa and repeated three times, and then argon was charged at atmospheric pressure. Subsequently, the crucibles containing molten Si and slag were cooled down to room temperature at a rate of 10 K/min. The refined Si was separated with slag use physical method and ground to powder for ICP-MS analysis to quantify the P content. The partition ratio of P between Si and slag was calculated by the ratio of P content in slag to P content in Si. The refining results are shown in Table 2. To

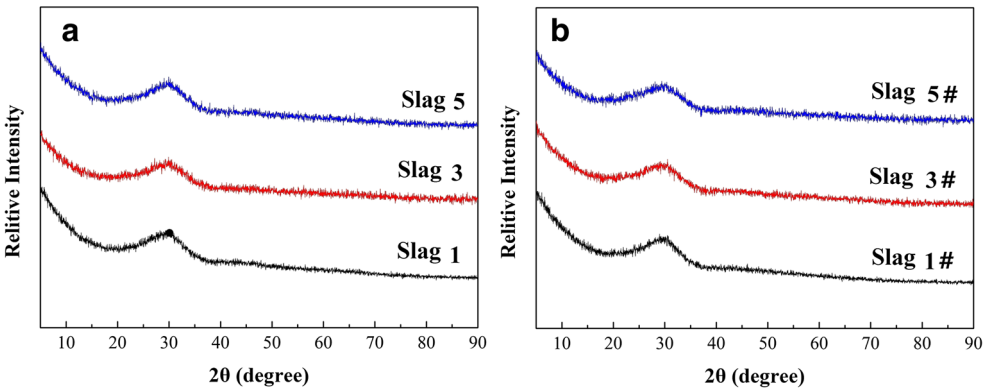

Fig. 2 XRD Curves of the Quenched Samples. **a** without P_2O_5, **b** 5 wt% P_2O_5

determine the role of Fe^{2+} and Fe^{3+} in P removal, another two slags with addition of 2.5% and 5% Fe_2O_3 were selected for refining. The experimental conditions during refining are consistent with the above. The results are plotted in Fig. 3.

The activity of dissolved oxygen in molten Si ($a_{[O]}$) was measured to denote the oxygen potential. To definite the value of $a_{[O]}$ at the equilibrium state during refining, three groups of refining experiment (slags containing 0, 5.36 wt%, 9.25 wt% FeO, respectively) were measured using electro motive force (EMF) method [49], recording equipment, an oxygen probe and sampling tubes, where zirconia is used as a matrix and magnesium oxide as a solid electrolyte. When system had reached equilibrium state at 1823 K, an oxygen probe was inserted into the molten Si inside the crucible and then the recording equipment was used to record the electro motive force. The EMF value was obtained within five seconds after immersion. Then, the stable EMF value and temperature were recorded.

2.3 Measurements of Raman Spectroscopy and ^{31}P MAS-NMR Spectroscopy

To clarify the structural characteristics of phosphosilicate melts, the Raman spectroscopy were employed to investigate the structural role of P_2O_5 in slag melts (two groups: with and without addition of 5 wt% P_2O_5). A laser Raman spectrometer (LabRAM HR800, Raman) was performed with an excitation wavelength of 532 nm and a 1 mW semiconductor laser as the light source for Raman test. The spectra of the samples were recorded in the frequency range from 400 to 2000 cm^{-1} and the precision of wave number is 1 cm^{-1} at room temperature. To further identify the specific structural units in the glasses, solid-state ^{31}P MAS-NMR measure was performed using a 500-M solid NMR spectrometer (Bruker Advance III HD 500 MHz) with a MAS probe of a 4⁻mm ZrO_2 rotor and two pairs of Dupont Vespel caps.

Table 2 Proportion of Fe^{2+} and Fe^{3+} and the content of FeO and Fe_2O_3 pre-melting in CaO-SiO_2-Al_2O_3-Fe_xO slags, %

No.	Fe_xO wt%	Fe^{2+}		Fe^{3+}		L_P
		Fe^{2+}, %	FeO, wt%	Fe^{3+}, %	Fe_2O_3, wt%	
1	0	–	0	–	0	1.06
2	2.86	66.65	1.91	33.35	0.95	1.58
3	8.78	61.11	5.36	38.89	3.42	1.95
4	12.64	62.32	7.87	37.68	4.77	1.65
5	14.51	63.72	9.25	36.28	5.26	0.95

3 Result and Discussion

3.1 Determination of Fe^{2+} and Fe^{3+} in Slag and its Effect on P Removal

Figure 3 shows the effect of FeO and Fe_2O_3 on the removal of P, it can be seen that the remained P in Si decreases with increasing FeO, however, the addition of Fe_2O_3 leads to the increase of phosphorous. It is apparent known that the FeO is beneficial for phosphorous removal rather than Fe_2O_3 that is harmful to P

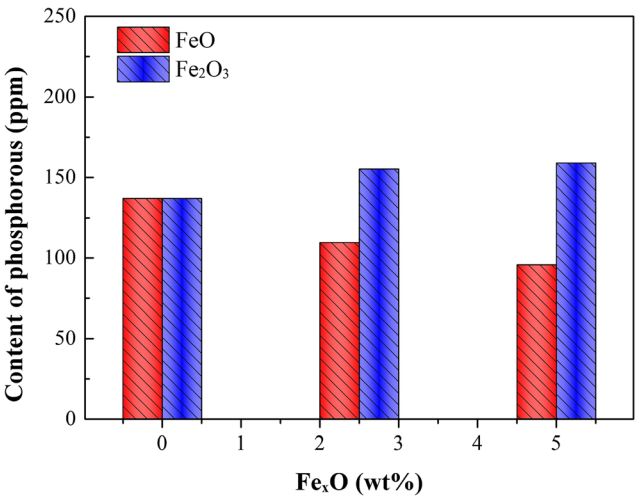

Fig. 3 The phosphorous content in Si after refining using CaO-SiO_2-Al_2O_3-Fe*x*O slag

removal. Therefore, it is deemed appropriate to attempt to quantify and account for the proportion of FeO in slags.

Figure 4 shows the XPS spectra of $CaO–SiO_2–Al_2O_3–Fe_xO$ slag with initial addition Fe_xO of content of each slag. It can be seen that both Fe^{2+} and Fe^{3+} of Fe_xO exist in slag due to insufficient atmosphere protection. The least squares method was used to fit the spectra to the spectrum. According to the references XPS spectra of FeO and Fe_2O_3 [34–38], $2p_{3/2}$ of line designation with about 710 eV binding energy correspond to iron (II) oxide (FeO), and the peaks near 725 eV correspond to $Fe_{2p\ 1/2}$ of Diiron trioxide (Fe_2O_3), as shown in Table 3. Using Gaussian fitting formula to integrate the peak areas of Fe^{2+} and Fe^{3+}, the proportion of Fe^{2+} and Fe^{3+} in each slag can be determined by area ratio and the results are shown in Table 2. It can be seen that the proportion of Fe^{2+} basically changed around 60%, the content of FeO varied from 0 to 9.25 wt%. Based on the determination of FeO in slags, further studies of the effect of FeO on the partition ratio of phosphorous will be carried out in the following section.

3.2 Effect of FeO on the Partition Ratio of Phosphorous

The experimental results for the equilibrium of pre-melting Si with $CaO–SiO_2–Al_2O_3–FeO$ slag are summarized in Table 2, and the values of L_P are plotted in Fig. 5. The works of dephosphorization from molten steel using refining slag containing FeO, obtained by Nagabayashi et al [21], Fengshan Li et al [22] and Danaei et al [23] were selected to compare with the present study due to the lack of information about refining of Si using FeO-related slag systems. As observed in Fig. 5, it is clearly to see that the partition ratios of phosphorous all show a tendency of increase first and then decrease as adding FeO. In present $CaO–SiO_2–Al_2O_3–FeO$ quaternary system with a basicity of 1, a lower FeO content (0~10.63 wt%) can result in obvious change of L_P and its value reaches the maximum of 1.95 at the FeO content of 5 ± 0.1 wt%. A higher FeO content (5~30 wt%) is required for the $FeO–CaO–SiO_2$ ternary system when basicity is more than 2 in the work of Nagabayashi et al [21]. However, the change of L_P value becomes insignificant in $CaO–SiO_2–Al_2O_3–Na_2O–TiO_2–FeO$ complex slag system [22, 23], although the FeO content increases from 20 to 50 wt%. The above results present the complex influence of FeO on L_P.

3.3 Dependence of the Partition Ratio of Phosphorous on Oxygen Potential

The calculation results of FeO activity with FactSage 6.3 as a function of the partition ratio of phosphorous were plotted in Fig. 6. It can be seen that higher FeO addition in slag does result in the increase of the activity of FeO, and a FeO activity value of 1.28 is obtained when FeO content reaches about 10 wt%. It's worth noting that the increase of FeO activity is unable to lead to that the value of L_P is increasing, L_P value presents a decrease trend when FeO activity is more than

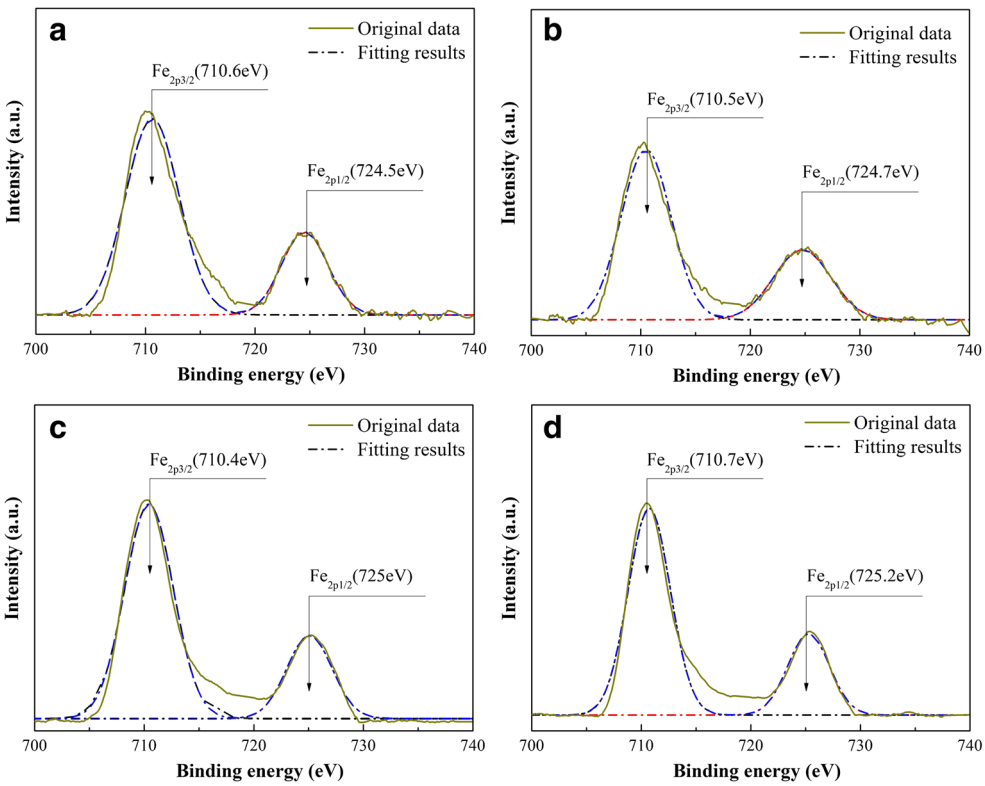

Fig. 4 XPS Spectra of CaO-$SiO^{2-}Al_2O3$-FeO Slag with Initial Addition FexO of Content of in Each Sample. **a** 2.86 wt%, **b** 8.78 wt%, **c** 12.64 wt%, **d** 14.51 wt%

Table 3 Matches from Fe element and available photoelectron line(s)

Formula	XPS formula	Line designation	Binding energy(eV)	References
FeO	Iron(II) oxide	$2p_{3/2}$	709.4	[34]
FeO	Iron(II) oxide	$2p_{3/2}$	709.9	[35]
FeO	Iron(II) oxide	$2p_{3/2}$	710.7	[36]
Fe_2O_3	Diiron trioxide	$2p_{1/2}$	724.2	[37]
Fe_2O_3	Diiron trioxide	$2p_{1/2}$	725.0	[38]

about 5 ± 0.1%. According to the original design, the addition FeO was used to improve the oxidation capacity of the slag. Therefore, the relationship between the oxygen activity of molten Si and FeO activity of slag was further studied.

The Mo + MoO_2 oxygen probes were used for the oxygen activity measurements in the present study. The equation as follows:

$$\ln a_{[O]} = \frac{\Delta G^{\theta}}{RT} - \frac{nF}{RT}E \tag{3}$$

where, E is the EMF measured with calibration, volt; R is the gas constant, 8.314 J/K/mol; F is the Faraday constant 96,500 J/V/mol; T is the molten Si temperature, K. $a_{[O]}$is the activity of dissolved oxygen that can be obtained as follows equation:

$$\lg a_{[O]} = 3.885 - \frac{7725 - 10.08E}{T} \tag{4}$$

The calculated $a_{[O]}$ value and activity of FeO are plotted in Fig. 7. As can be seen, the $a_{[O]}$ value and activity of FeO present a linear increase, indicating higher FeO activity can promote the increase of the oxygen potential. It is generally believed that the increase of oxygen potential is beneficial to the removal of P. The issue is that the removal efficiency of phosphorous decreases when FeO content exceeds 5 ± 0.1 wt%, although under a condition of higher oxygen potential. It could be speculated that oxygen potential is not the only factor to affect P removal. Besides, the oxygen ion introduced by FeO in slag might play an important role in the removal of phosphorous. In addition, oxygen ions are directly related to the structure of slag, such as the behavior and state of P and Si in slag. Therefore, in the following sections, the behavior and state of P and Si in slag due to increase of oxygen ions and its correlation with P removal will be further studied based on the investigation of slag structure using Raman spectroscopy and ^{31}P MAS NMR spectroscopy.

3.4 Behavior and Stability of P in Slag by Raman and ^{31}P NMR Spectroscopy

The basis of the coordination environment is the silicate network, and it can be characterized by the bridging oxygen (BO) and non-bridging oxygen (NBO) in each SiO_4 polyhedron [21–23]. Basic oxide can destroy the silicate network to produce Q^n units (Q^n refers to Si with n BOs and 4–n NBOs) [25, 26]. A BO connects two adjacent polyhedra, such as Si–O–Si and Si–O–P, determining the connectivity of silicate and phosphate network. The oxygen in the bridge oxygen can be thought of as O^0 because both bonds are compensated by Si and P anions. For a NBO, it can connect a polyhedra and cation by the form of Si–O–Ca and P–O–Ca, denoting a fragmented phosphosilicate networks. The oxygen in the non-bridge oxygen can be thought of as O^- because only one bond is compensated by Si or P anion. Free oxygen ions (O^{2-}), bridged oxygen and non-bridged oxygen have this relationship as shown in Eq. (5). Therefore, the introduction of free oxygen ions can lead to the change of relative quantity of BO and NBO.

$$O^{2-} = O^0 + 2O^- \tag{5}$$

In general, the Q^n distributions can often be obtained directly through Raman spectra and the Raman spectroscopy of the $CaO–SiO_2–Al_2O_3–Fe_xO$ slags were investigated. The Raman spectra of quaternary system $CaO–SiO_2–Al_2O_3–Fe_xO$ glasses

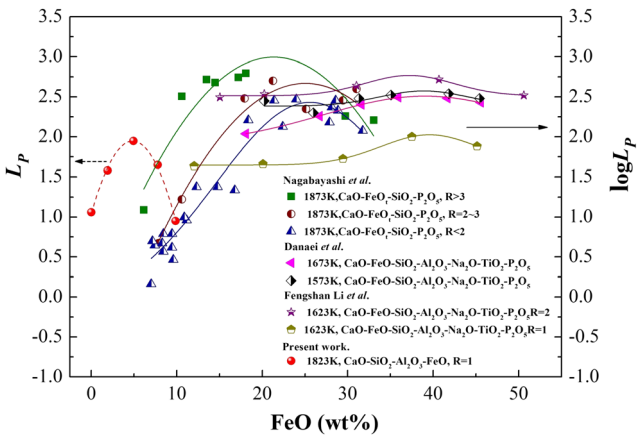

Fig. 5 *LP* values as a function of FeO content for different slag composition

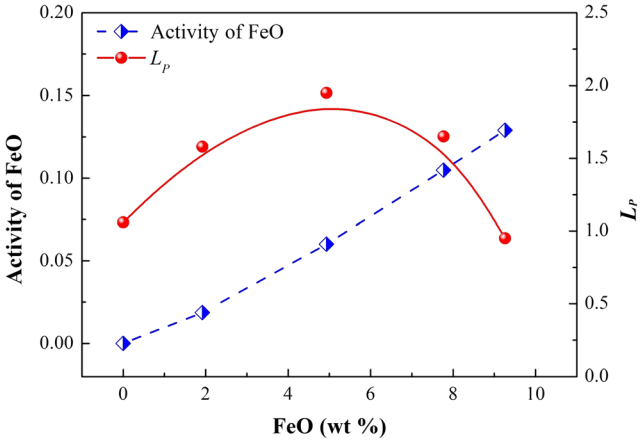

Fig. 6 Effect of FeO content on the partition ratio of phosphorous and FeO Activity

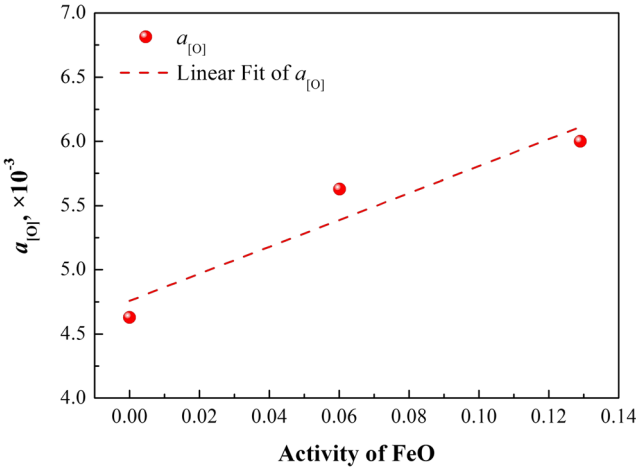

Fig. 7 Activity of dissolved oxygen ($a_{[O]}$) as a function of the activity of FeO in slag

were deconvolved using Gauss-deconvolution method with the minimum correlation coefficient as $r^2 \geq 0.995$, as shown in Fig. 8. A number of works report that the major peaks near 870 cm^{-1}, 960 cm^{-1}, 990 cm^{-1}, and 1050 cm^{-1} could be assigned to the monomer structure (Q^0), the dimer structure (Q^1), Q^2, and Q^3 [29–32], which were employed to deconvolute the Raman curves and the deconvolution results of Q^n species based on the Raman spectra are presented in Fig. 8. It can be seen that in the group of Fig. 8a, b, c, there are three kinds of species under the condition of FeO content less than or equal to 5 ± 0.1 wt% in (a), (b), namely, Q^0, Q^2, and Q^3, of which Q^2 are the main species. The peak intensity of Q^3 weakens with the increase of FeO content. After the addition of P_2O_5 (Fig. 8e, f, g), we can see there are also three kinds of species namely, Q^0, Q^2, and Q^3, where Q^2 and Q^3 are the main species and the peak intensity of Q^3 gets enhanced compared with slags without P_2O_5. When FeO content is about 5 ± 0.1 wt%, there is a new peak of Q^1 around 890 cm^{-1} chemical shift and it becomes greater with the further increase of FeO content (Fig. 8f, g).

The relative abundance of Q^n ($n = 0$ to 3) species can be obtained by calculating the area ratio of an individual species, the fitting results as shown in Fig. 9. For CaO–SiO_2–Al_2O_3–Fe_xO slag, it is noted that relative abundance of Q^0 and Q^2 increase at the expense of Q^3 population as the FeO content increasing to about 10 wt%, indicating FeO can depolymerize silicate network in the role of basic oxides.

When 5 wt% P_2O_5 was added, Q^0 and Q^2 proportion decrease obviously while the relative abundance of Q^1 and Q^3 increase. P_2O_5 can involve in removing the ferrous ion and calcium ions from the silicate network to achieve the charge balance of the orthophosphate groups, since Na^+ and Ca^{2+} ions prefer to charge balance orthophosphate rather than the silica [48]. moreover, the greater stability of P–O–M than of Si–O–M bonds [41], the former bonds would be favored, thus resulting in polymerization of silicate portion of the melt. As did Mysen et al [42], it is suggested that the following reaction takes place:

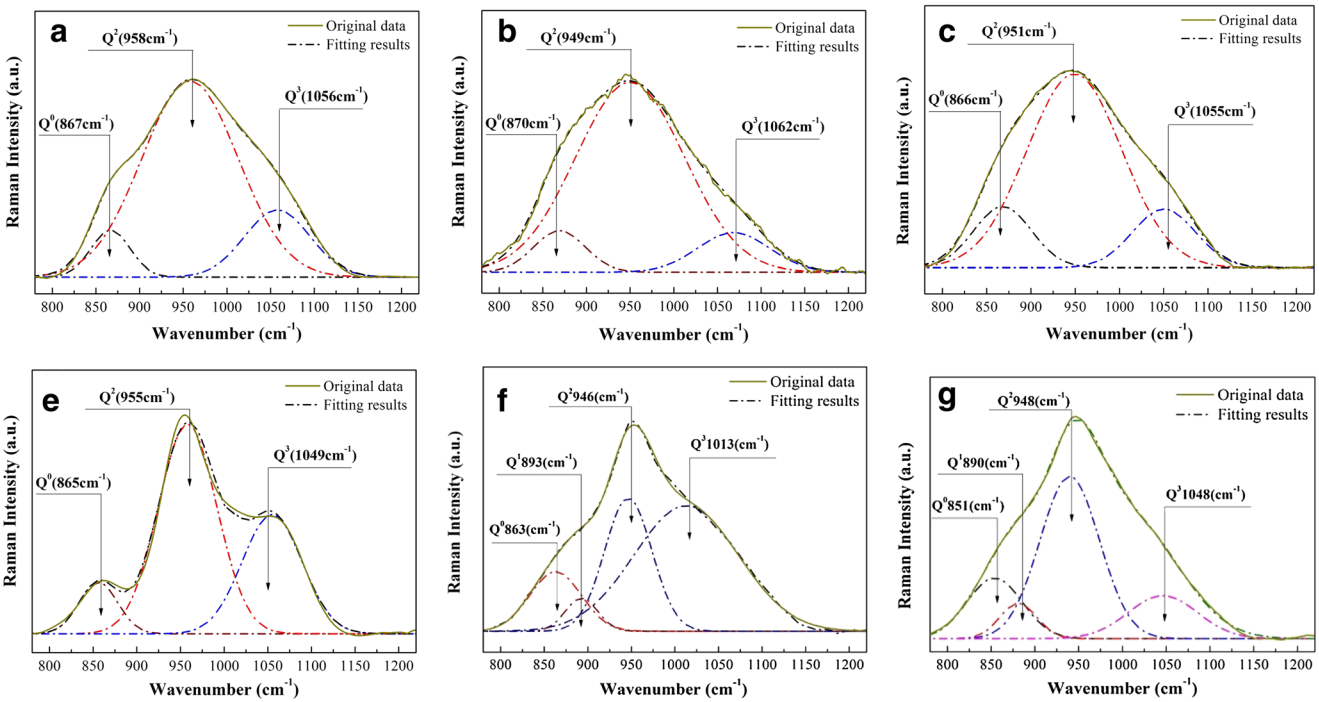

Fig. 8 Room-temperature Raman Spectra of CaO-SiO_2-Al^2O3-FexO Slag of (**a**) 0 FeO, **b** 5.36 wt% FeO, **c** 9.25 wt% FeO, **e** 0 FeO and 5wt%P_2O_5, **f** 5.36 wt% FeO and 5wt%P_2O_5, **g** 9.25 wt% FeO and 5wt%P_2O_5

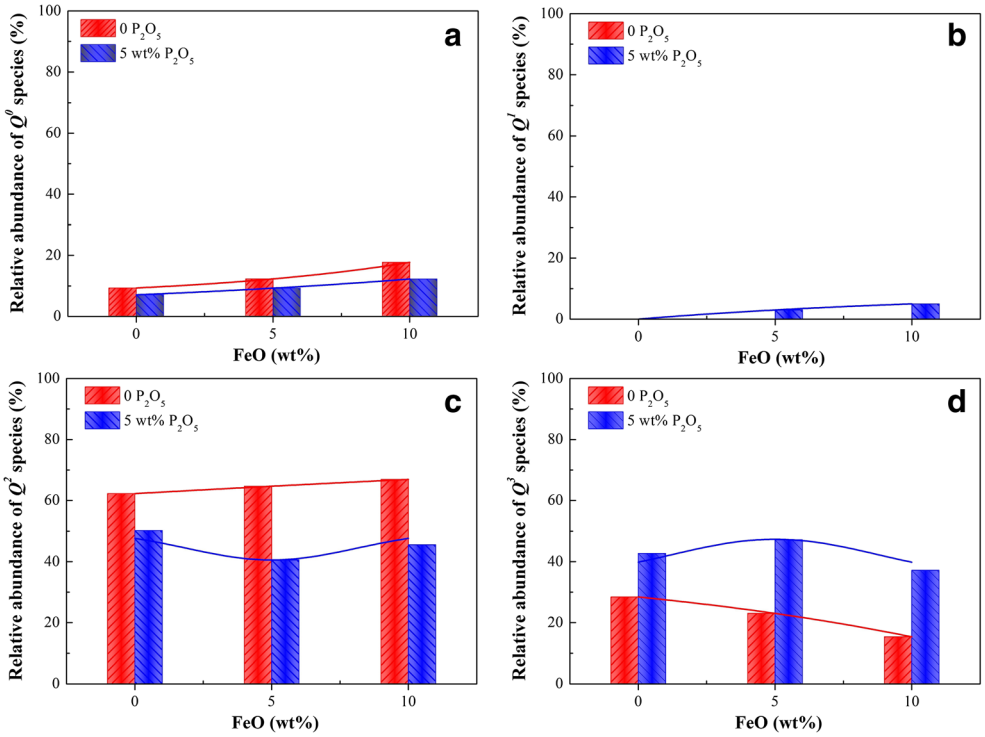

Fig. 9 Relative Abundance of Qn ($n = 0$ to 3) Species as a Function of FeO content. **a** Q^0, **b** Q^1, **c** Q^2, **d** Q^3

$$\mathrm{O^0-P=O^0 + 2M-O^- -Si-} \rightleftarrows \mathrm{O^0-P-O^-M+ -Si-O-Si-O^- -M} \quad (6)$$

In this process, a nonbridging oxygen (O^-) in the silicate network is lost and a new bridging oxygen (O^0) is formed by the formation of the metal (M) phosphate complex. The proportions of sheets (Q^3) increase relative to that of chain (Q^2) and monomer (Q^0).

Q^0~Q^3 can reveal the bridge oxygen and non-bridge oxygen in different Si–O structures, the average bridge oxygen content and non-bridge oxygen content could be represented by Eq. (7) [28] and Eq. (8) [43], respective. The concentration of O^{2-} provided by the addition of FeO can be represented by the mole fraction of O^{2-}. Bridge oxygen (BO) value and non-bridge oxygen (NBO) value as a function of the mole fraction of O^{2-} of FeO is shown in Fig. 10.

$$\mathrm{BO} = 0 \times Q^0 + 1 \times Q^1 + 2 \times Q^2 + 3 \times Q^3 \quad (7)$$

$$\mathrm{NBO} = 4 \times Q^0 + 3 \times Q^1 + 2 \times Q^2 + 1 \times Q^3 \quad (8)$$

Figure 10 shows the effect of the mole fraction of O^{2-} from FeO addition on the values of NBO and BO. As expected, the addition of P_2O_5 in slag leads to the reduction of NBO and the increase of BO because that P_2O_5 is a network body. For the effect of O^{2-}, it can be seen that increasing the mole fraction of O^{2-} can lead to the increase of NBO value of CaO–SiO_2–Al_2O_3–Fe_xO slag and CaO–SiO_2–Al_2O_3–Fe_xO–P_2O_5 slag, oppositely, BO value shows the decrease trend. Especially when O^{2-} mole fraction is higher than 0.04, NBO value increases rapidly. According to Eq. (5), the raise of O^{2-} concentration promotes the reaction to the right. O^- has a higher stoichiometric ratio of 2 relative to O^0, thus more amount of O^- tends to be produced. Therefore, it can be known that the Raman structure result in

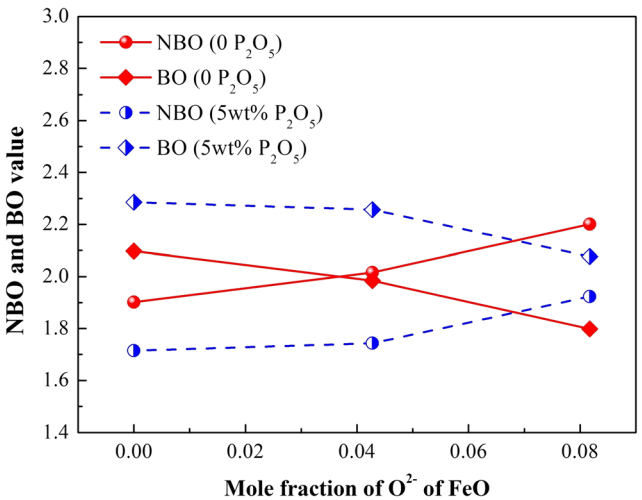

Fig. 10 NBO and BO value as a function of mole fraction of O^{2-} of FeO in CaO-SiO2-Al2O3-FexO slag and CaO-SiO2-Al2O3-FexO-P2O5 slag

Fig. 10 agree with the reaction of Eq. (5), indicating FeO mainly play a role in depolymerization of the network.

In order to illuminate the effect of NBO on the stability of P in silicate networks, the relative abundance of Q^2 and Q^3 of CaO–SiO_2–Al_2O_3–Fe_xO–P_2O_5 slag as a function of NBO value was studied, as shown in Fig. 11. It can be seen that as NBO value increases from 1.70 to 1.75, the relative abundance of Q^3 species presents an increase, indicating some nonbridging oxygen (O^-) could promote the polymerization of phosphates and silicate, this phenomenon is consistent with the results of Mysen et al [42]. The introduce of a part of nonbridging along with oxygen some metal cation helps to compensate for the charge of P_2O_5, which provides the possibility of combining phosphate with silicate network bodies. It is believed that Q^2 in silicate network can transforms into Q^3(Si and P) by capturing PO_4^{3-} that from the charge compensation of P_2O_5 by O^{2-}. Moreover, the relative abundance of Q^3 species shows rapid decrease when NBO value increases to move than 1.92, indicating the stability of P in silicate networks is destroyed. Therefore, the specific structural unit of P and the combination between P and silicate network was further described in the following.

The chemical environments of the P atoms were examined using ^{31}P MAS NMR on a home-built 500–MHz spectrometer, the results as shown in Fig. 12. The resonances with the chemical shift in the range 1.0–10 ppm in Fig. 5 are most probably the characteristic of orthophosphate, and it has the greater the relative proportions of peaks [40, 46]. A number of works reported that PO_4 groups are predominantly isolated as orthophosphates for the glasses containing less than 10% P_2O_5 amounts [39, 40], which is satisfied for

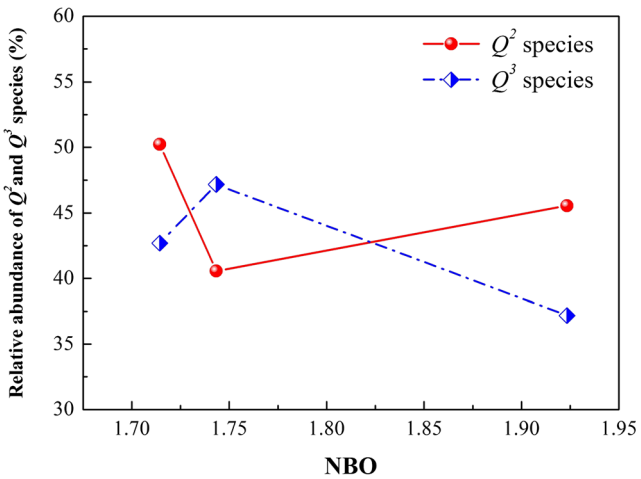

Fig. 11 Relative abundance of Q^2 and Q^3 as a function of NBO value in CaO-SiO2-Al2O3-FexO-P2O5 slag

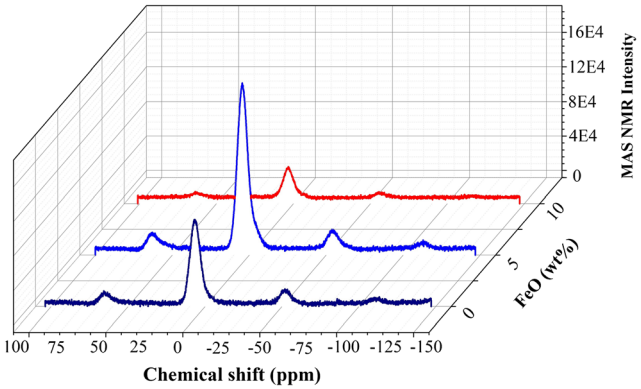

Fig. 12 ^{31}P MAS-NMR Spectra of CaO-SiO2-Al2O3-FexO-P2O5 slag

corresponds to the conjecture in Eq. (6) and the Raman results in Fig. 9.

In addition, the ^{31}P spectra shows an peak at about −50 ppm consistent with the P environment in SiP_2O_7 where all P–O bonds are bridging, which is satisfied for the study in ref. 47. Whilst there is a feature to be seen in the range of −110 – −120 ppm chemical shifts, indicating that P–O–Si bond now occurs [39, 47]. These evidences confirm the link between phosphates and silicates and this connection has also been found in number of silicates, for example, E. Tillmanns et al [44] and D. M. Poojary et al [45] reported the P–O–Si bonds are found in crystalline SiP_2O_7 and $Si_5O(PO_4)_6$, Respectively. Therefore, it can be speculated that a fraction of P can be incorporated into the silicate network, which will limit the mobility by forming P–O–Si bonds. However, for the slag with about 10 wt% FeO, the peak of P–O–Si bonds get very small relative to the other two peaks, which is consistent with the result that larger NBO value (more than 1.92) can destroy the stability of P in silicate network in Fig.11.

3.5 Role of FeO on the Removal of Phosphorous during Slag Refining Process of Si

According to the purpose of adding FeO into slag, it can provide both the oxygen potential and the oxygen ion potential to strengthen the removal of P from Si. Above results show that the increase of FeO can raise the dissolved oxygen content in molten Si and the mole fraction of O^{2-} in slag, where O^{2-} also promotes the formation of non-bridged oxygen. In order to clearly compare the effects of oxygen potential and oxygen ion potential on P removal, the values of $a_{[O]}$, NBO and L_P as a function of FeO content are plotted in Fig. 13. Moreover, a schematic diagram of mechanism was drawn to visualize the role of these factors in removing P during slag refining process, as shown in Fig. 14. It can be seen from Fig. 13 that the values of $a_{[O]}$ and NBO both increase as increasing FeO content,

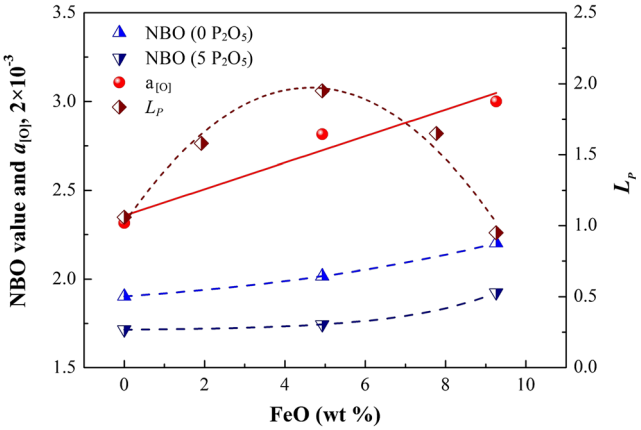

Fig. 13 Values of a[O], NBO and *LP* as a function of FeO content for in CaO-SiO2-Al2O3-FexO slag and CaO-SiO2-Al2O3-FexO-P2O5 slag

but L_P value presents first increase and then decrease trend. It is well known that free oxygen activity is beneficial to the removal of P. Previous study [27] has shown that NBO is necessary for the combination of boron and silicate network, but it can break both bonding when it exceeds a certain amount.

When FeO content is added to less than 5 ± 0.1 wt% corresponding to the left of Fig. 14, it can be known that the P in the molten Si is oxidized by the dissolved oxygen to form P_2O_5, and then P_2O_5 evolves into phosphate (PO_4^{3-}) through the charge compensation of free oxygen (O^{2-}) at the interface of slag and Si. Subsequently, PO_4^{3-} is captured by Q^0 and Q^2 to achieve the incorporation P into silicate network by the form of $Q^1$and Q^3. Based on results of Fig. 8, Q^3 (Si and P) is the main form of structure. Therefore, it can be believed that the increase of NBO and $a_{[O]}$ can promote the removal of P as FeO content is less than 5 ± 0.1 wt%, so the L_P value shows an increase trend with the increase of FeO content in Fig. 13.

For the condition of FeO content is more than 5 ± 0.1 wt%, L_P value gradually decreases although the values of NBO and $a_{[O]}$ are increasing in Fig. 13. It can be seen from the right of Fig. 14 that more NBO can depolymerize the Q^3 (Si and P) to destroy the stability of P in silicate network. As a result, a mount of PO_4^{3-} is present at the interface to prevent the oxidation of phosphorous, although the activity of dissolved oxygen is increasing.

4 Conclusions

(1) With increasing FeO content from 0 to 9.26 wt%, the removal ratio of phosphorous from Si first increases and then decreases. The maximum value is obtained when the FeO content is 5 ± 0.1 wt%.

(2) The addition of FeO into slag can promote the increase of oxygen potential in molten Si. The activity value of dissolved oxygen increases from about 4.5×10^{-3} to more than 6×10^{-3} in the process of FeO content increase to about 10 wt%. The increasing activity of FeO in slag is the key to improve the oxygen potential.

(3) Q^0, Q^1, and Q^2 of the Si network play a role in capturing phosphorous in slag. Phosphorous mainly combines with the non-bridge oxygen of Q^2 to form Q^3(Si and P) if the FeO content is less than 5 ± 0.1 wt%. In this case, the Q^3(Si and P) is the final sable structure for fixing phosphorous. However, when the FeO content exceeds 5 ± 0.1 wt%, Q^3(Si and P) is depolymerized by excessive NBO converted from O^{2-} and the phosphorous fixed in the silicate network becomes unstable, which leading to the decrease of phosphorous removal ratio.

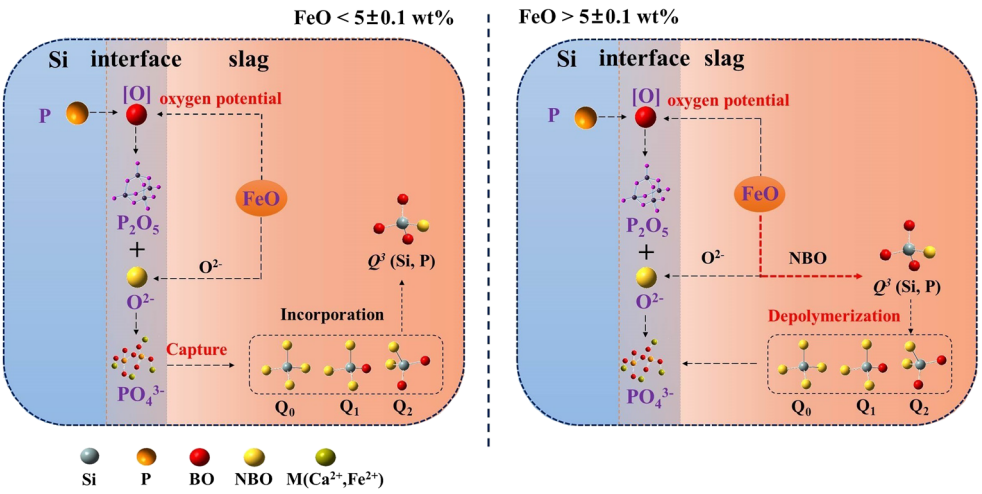

Figure 14 Mechanism of P removal from Si to slag under different condition of FeO content

Acknowledgements This work was financially supported by National Natural Science Foundation of China (Nos. 51604256 and U1702251), National Key R&D Program of China (2018YFC1901801) and Beijing Natural Science Foundation (2192055).

References

1. Luque A, Hegedus S (2003) Handbook of photovoltaic science and engineering. Wiley Ltd, New York Chapter 5
2. Sarti D, Einhaus R (2002) Silicon feedstock for the multi-crystalline photovoltaic industry. Sol Energ Mat Sol C 72:27–40
3. Sergiienko SA, Pogorelov BV, Daniliuk VB (2014) Silicon and silicon carbide powders recycling technology from wire-saw cutting waste in slicing process of silicon ingots. Sep Purif Technol 133:16–23
4. Hachichi K, Lami A, Zemmouri H, Cuellar P, Soni R, Ait-Amar H, Drouiche N (2018). Silicon 10:1579–1589
5. Pushpavanam M, Manikandan H, Ramanathan K (2007) Preparation and characterization of nickel–cobalt-diamond electro-composites by sediment co-deposition. Surf Coat Technol 201:6372–6379
6. Liu S, Huang K, Zhu H (2016) Removal of Fe, B and P impurities by enhanced separation technique from silicon-rich powder of the multi-wire sawing slurry. Chem Eng J 299:276–281
7. Lu T, Tan Y, Li J, Deng D (2018) Recycling of silicon powder waste cut by a diamond-wire saw through laser-assisted vacuum smelting. J Clean Prod 203:574–584
8. Tomono Z, Miyamoto S, Ogawa T, Furuya H, Okamura Y, Yoshimoto M, Komatsu R, Nakayama M (2013) Recycling of kerf loss silicon derived from diamond-wire saw cutting process by chemical approach. Sep Purif Technol 120:304–309
9. Lin Y, Wang T, Lan C, Tai CY (2010) Recovery of silicon powder from kerf loss slurry by centrifugation. Powder Technol 200:216–223
10. Wang TY, Lin YC, Tai CY, Sivakumar R, Rai DK, Lan CW (2008) A novel approach for recycling of kerf loss silicon from cutting slurry waste for solar cell applications. J Cryst Growth 310:3403–3406
11. Jia G, Plentz J, Gawlik A, Azar AS, Stokkan G, Syvertsen M, Carvalho PA, Dellith J, Dellith A, Andrä G, Ulyashin A (2016). Int J Photoenergy 19:7582–7589
12. Suzuki K, Kumagal T, Sano N (1992) Removal of boron from metallurgical-grade silicon by applying the plasma treatment. ISIJ Int 32:630–634
13. Ikeda T, Maeda M (1992) Purification of metallurgical silicon for solar-grade silicon by electron beam button melting. ISIJ Int 32:635–642
14. Momokawa H, Sano N (1982) The effect of oxygen potential on phosphorus in the CaO−Al2O3 system. Metall Mater Trans B Process Metall Mater Process Sci 13:643–644
15. Tanahashi M, Fujisawa T (2013). Metall Mater Trans B Process Metall Mater Process Sci 45:629–642
16. Jung EJ, Moon BM, Min DJ (2011) Quantitative evaluation for effective removal of phosphorus for SoG-Si. Sol Energy Mater Sol Cells 95:1779–1784
17. Johnston M, Barati M (2010) Distribution of impurity elements in slag–silicon equilibria for oxidative refining of metallurgical silicon for solar cell applications. Sol Energ Mater Sol Cells 94:2085–2090
18. Teixeira LAV, Morita K (2009) Removal of boron from molten silicon using CaO–SiO2 based slags. ISIJ Int 49:783–787
19. Wu JJ, Wang FM, Ma WH (2016) Thermodynamics and kinetics of boron removal from metallurgical grade silicon by addition of high basic potassium carbonate to calcium silicate slag. Metall Mater Trans B Process Metall Mater Process Sci 47:1796–1803
20. Krystad E, Tang K, Tranell G (2012). JOM. 64:968–972
21. Li FS, Li XP, Yang SF (2017) Distribution ratios of phosphorus between CaO-FeO-SiO2-Al2O3/Na2O/TiO2 slags and carbon-saturated iron. Metall Mater Trans B Process Metall Mater Process Sci 48:2367–2378
22. Nagabayashi R, Hino M, Ban-Ya S (1989) Mathematical expession of phosphorus distribution in steelmaking process by quadratic formalism. ISIJ Int 29:140–147
23. Danaei A, Yang YD, Barati MC, Ravindran R (2013). Mater Sci Technol 27 CD only
24. Pak JJ, Fruehan RJ (1986) Soda slag system for hot metal dephosphorization. Metall Mater Trans B Process Metall Mater Process Sci 17:797–804
25. Yang XM, Shi CB, Zhang M (2011) A thermodynamic model of phosphate capacity for CaO-SiO2-MgO-FeO-Fe2O3-MnO-Al2O3-P2O5 slags equilibrated with molten steel during a top–bottom combined blown converter steelmaking process based on the ion and molecule coexistence theory. Metall Mater Trans B Process Metall Mater Process Sci 42:951–977
26. Morales AT, Fruehan RJ (1997) Thermodynamics of MnO, FeO, and phosphorus in steelmaking slags with high MnO contents. Metall Mater Trans B Process Metall Mater Process Sci 28:1111–1118
27. Qian GY, Wang Z, Gong XZ (2017) The importance of slag structure to boron removal from silicon during the refining process: insights from raman and nuclear magnetic resonance spectroscopy study. Metall Mater Trans B Process Metall Mater Process Sci 48:3239–3250
28. Teixeira LAV, Tokuda Y, Yoko T, Morita K (2009) Behavior and state of boron in CaO–SiO2 slags during refining of solar grade silicon. ISIJ Int 49:777–782
29. Tsunawaki Y, Iwamoto N, Hattori T, Mitsuishi A (1981) Analysis of CaO · SiO2 and CaO · SiO2 · CaF2 glasses by Raman spectroscopy. J Non-Cryst Solids 44:369–378
30. Sun YQ, Zhang ZT (2015). Metall Mater Trans B Process Metall Mater Process Sci 46B:1549–1554
31. Seifert FA, Mysen BO, Virgo D (1982). Am Mineral 67:696–717
32. Tan J, Zhao SR, Wang WF (2004) The effect of cooling rate on the structure of sodium silicate glass. Mater Sci Eng B 106:295–299
33. Wang ZJ, Shu Q (2015) Effect of P2O5 and FetO on the viscosity and slag structure in steelmaking slags. Metall Mater Trans B Process Metall Mater Process Sci 46:758–765
34. McIntyre NS, Zetaruk DG (1977) X-ray photoelectron spectroscopic studies of iron oxides. Anal Chem 49:1521–1529
35. Hawn DD, DeKoven BM (1987) Deconvolution as a correction for photoelectron inelastic energy losses in the core level XPS spectra of iron oxides. Surf Interface Anal 10:63–74
36. Mills P, Sullivan JL (1983) A study of the core level electrons in iron and its three oxides by means of X-ray photoelectron spectroscopy. J Phys D Appl Phys 16:723–732
37. Langevoort JC, Sutherland I, Hanekamp LJ, Gellings PJ (1987) On the oxide formation on stainless steels AISI 304 and incoloy 800H investigated with XPS. Appl Surf Sci 28:167–179
38. Tan BJ, Klabunde KJ, Sherwood PA (1990) X-ray photoelectron spectroscopy studies of solvated metal atom dispersed catalysts. Monometallic iron and bimetallic iron-cobalt particles on alumina. Chem Mater 2:186–191
39. Lockyer MWG, Holland D, Dupree R (1995) NMR investigation of the structure of some bioactive and related glasses. J Non-Cryst Solids 188:207–219
40. Fayon F, Massiot D, Suzuya K, Price DL (2001) 31P NMR study of magnesium phosphate glasses. J Non-Cryst Solids 283:88–94

41. Tilocca A, Cormack AN, de Leeuw NH (2007) The Structure of Bioactive Silicate Glasses: New Insight from Molecular Dynamics Simulations. Chem Mater 19:95–103
42. Mysen BO, Ryerson FJ, Virgo D (l981). Am Mineral 66:106–117
43. Kline J, Tangstad M, Tranell G (2015). Metall Mater Trans B Process Metall Mater Process Sci 46B:62–73
44. Tillmanns E, Gebert W, Baur WH (1973). J Solid State Chem 7:69–84
45. Poojary DM, Borade RB, Campbeii III FL, Clearfield A (1994). J Solid State Chem 112:106–112
46. Elgayar I, Aliev AE, Boccaccini AR, Hill RG (2005) Structural analysis of bioactive glasses. J Non-Cryst Solids 351:173–183
47. Dupree R, Holland D, Mortuza MG, Collins JA, Lockyer MWG (1989) Magic angle spinning NMR of alkali phospho-alumino-silicate glasses. J Non-Cryst Solids 112:111–117
48. Tilocca A, Cormack AN (2007) Structural effects of phosphorus inclusion in bioactive silicate glasses. J Phys Chem B 111:14256–14264
49. Martynov PV, Chernov ME, Levskit VA (2005). Atom Energy 98: 343–346